Applied Catalysis B: Environmental 183 (2016) 386–393

Contents lists available at ScienceDirect

Applied Catalysis B: Environmental

journal homepage: www.elsevier.com/locate/apcatb

Direct electrochemical oxidation of ethanol on SOFCs: Improved carbon tolerance of Ni anode by alloying

Brittany Farrell, Suljo Linic*

Department of Chemical Engineering, University of Michigan, NCRC Building 28, 2800 Plymouth Rd, Ann Arbor, MI, USA

ARTICLE INFO

Article history:
Received 30 May 2015
Received in revised form 28 October 2015
Accepted 3 November 2015
Available online 7 November 2015

Keywords:
Solid oxide fuel cell
Ethanol
Tin
Ni/YSZ
Carbon deposition

ABSTRACT

Solid oxide fuel cells (SOFCs) are electrochemical devices that convert chemical energy in fuels into electrical energy through an electrochemical oxidation process. This technology is attractive since SOFCs can in principle utilize a range of combustible fuels including hydrogen, carbon monoxide, and hydrocarbons offering higher efficiencies than conventional electricity generators with limited emission of a number of common air pollutants such as NO_x and SO_x. The environmental efficiency of SOFC devices can further be improved by utilizing fuels that are more carbon-neutral (e.g., biofuels such as ethanol) than conventional fossil fuels. One of the problems with employing oxygenated liquid biofuels is that conventional Ni anode electro-catalysts deactivate due to carbon deposition on the surface of the anode during the process of electocatalytic fuel oxidation. We show that the stability of Ni SOFC anode electrocatalysts during electrochemical oxidation of ethanol is significantly improved when a small amount of Sn is introduced in the electrocatalyst design. The improvement in the stability is manifested in a more stable operation and higher kinetic currents of Sn/Ni compared to Ni electrodes under identical conditions with ethanol fuel. We discuss the underlying molecular mechanisms responsible for the enhanced stability of the anodes and propose a number of guiding principles for the design of carbon-tolerant anodes for oxidation of oxygenated hydrocarbons.

1. Introduction

Solid oxide fuel cells (SOFCs) are electrochemical devices that convert the chemical energy in fuels into electrical energy through an electrochemical oxidation process. SOFCs operate at temperatures ranging from ~800 to 1300 K. This technology is attractive since SOFCs can in principle utilize a range of combustible fuels including hydrogen, carbon monoxide, hydrocarbons, and oxygenated hydrocarbons, offering higher efficiencies than conventional electricity generators [1,2] with little to no emission of air pollutants [3] such as NO_x, and SO_x. Although SOFCs still emit CO_2 when operating on hydrocarbon fuels, the CO_2 effluent is physically separated from the air side of the fuel cell, and it must only be separated from water and excess fuel [4,5]. This ease of separation makes the technology compatible with the process of CO_2 capture and sequestration. The carbon footprint of SOFC devices can also be lowered by utilizing fuels that are more carbon-neutral (e.g., biofuels) than conventional fossil fuels. When made from biomass, fuels such as ethanol and butanol have greenhouse gas reductions of up to 60% compared to petroleum-based fuels [6,7]. These fuels are liquid at standard conditions and therefore also have additional benefits over gaseous fuels including high specific energy density and ease of storage and transport.

SOFCs can in principle directly utilize hydrocarbon and oxygenated hydrocarbon fuels, including ethanol and butanol which can be produced from biomass, without any pre-reforming of the fuel. While the direct operation simplifies the design of the SOFC system, it has been demonstrated that the stability of these cells is compromised due to high rates of carbon deposition on the conventional anode electrocatalysts, which contain nanometer to micrometer sized particles of Ni [1,8–13]. The carbon deposits take the form of graphitic carbon or carbon filaments. These deposits physically degrade the structure of the Ni anode [14–16]. Although carbon induced deactivation can occur with any fuel containing carbon, it has been reported that carbon deposition occurs more quickly for SOFCs operated on oxygenated hydrocarbons compared to alkanes [17]. It has been argued that the increase in carbon deposition for SOFCs operated on oxygenated fuels is caused by species produced by rapid gas phase pyrolysis of the fuel at temperatures relevant to operating SOFCs [17,18]. During the pyrolysis process many different compounds are formed, including acetylene and ethylene which are very potent in forming carbon deposits on the

* Corresponding author.
E-mail address: linic@umich.edu (S. Linic).

http://dx.doi.org/10.1016/j.apcatb.2015.11.002
0926-3373/

surface of the anode [17,19]. In contrast, methane, which is the fuel used in the majority of SOFC studies, is relatively stable and requires significantly higher temperatures to undergo rapid gas phase pyrolysis (>1273 K) [20]. Therefore, approaches that are effective at reducing or eliminating carbon deposition due to methane may not be effective when used with oxygenated hydrocarbons.

Several strategies have been employed to inhibit the formation of carbon deposits on SOFC anodes. One strategy is to add a pre-reformer which converts hydrocarbon fuels to carbon monoxide and hydrogen, which are then used as the fuel for SOFC [21,22]. These additions add complexity to the fuel cell system. Furthermore, an incomplete reformation of the fuel can lead to the leakage of hydrocarbon fuel to the cell and carbon-induced degradation of the cell. Another strategy is to add an oxidant, such as water or air, to the fuel to decrease the carbon to oxygen ratio on the anode and in doing so avoid operation at the conditions where carbon deposition is thermodynamically favored [19,23,24]. The problem with this approach is that in fuel cell systems it is often the kinetics of the carbon forming and degrading reactions that governs the stability, and carbon-induced anode deactivation has been observed even in systems where solid carbon is not the most thermodynamically favorable product [9]. Another issue with adding oxidants to the fuel is that it decreases the efficiency of the device by lowering the open circuit potential of the fuel cell. Furthermore, it has also been reported that water vapor can lead to sintering of the nickel in the anode lowering the rate of current generation (and therefore the power output) and decreasing the stability of the Ni anode [1]. A third strategy is to change the catalyst in the anode from Ni to a material that is less prone to carbon-induced deactivation. One approach is to utilize a composite containing Cu and CeO_2. It has been proposed that in these systems Cu functions as the electron conducting phase, while CeO_2 is the main catalyst for the conversion of hydrocarbons [8]. These systems show lower carbon deposit formation rates compared to the Ni anodes; however, they operate at lower temperatures which are required to prevent melting and sintering of the copper phase. Operating at lower temperatures offers some benefits since there are a larger number of the balance of plant materials that are stable under lower temperature conditions. However, the lower temperature operation decreases the reaction rates on the anode and the cathode sides as well as the flux of O^{2-} through the electrolyte. Another approach relies on the synthesis of Ni alloy electro-catalysts that exhibit physical properties similar to monometallic Ni while exhibiting improved carbon tolerance. For example, we have previously shown that the addition of a small amount of Sn to Ni anode catalysts creates a Sn/Ni surface alloy which showed improved tolerance to the carbon-induced deactivation with methane and isooctane fuels compared to fuel cells with monometallic Ni anodes [14,25,26]. These results have been supported by recent reports by Yoon and Kan and their respective coworkers [27,28].

In this contribution, we show that Ni electro-catalysts doped with a small amount of Sn (nominally 1% with respect to Ni) also show improved tolerance in electro-catalytic oxidation of oxygenated hydrocarbons (e.g., ethanol) compared to monometallic Ni anodes. Our conclusions are based on experimental observations that Sn doped Ni/YSZ anode fuel cells show less physical damage, less carbon deposition in the anode, and more stable electrochemical performance over time when compared to monometallic Ni anode fuel cells in electro-catalytic oxidation of ethanol. We note that oxygenated hydrocarbons such as ethanol are readily produced from biomass. In addition to reporting our experimental findings our results shed some light on the design principles that should guide the development of carbon-resistant SOFC anodes.

2. Experimental

2.1. Electrochemical measurements

Fuel cells used in this study were anode supported button cells with cathode areas of ~0.15 cm^2. The fuel cells were attached through the anode side directly onto the end of an alumina tube using alumina paste (Ceramabond 552), and fuel was fed via an inner tube perpendicular to the anode surface at atmospheric pressure. Gases were fed using either mass flow controllers or rotometers, and liquid fuels were fed using a bubbler at room temperature entrained by argon. Feed lines were heated to at least 373 K to avoid condensation of liquid fuels. The fuel cell cathode on the opposite side was open to the atmosphere. Electrochemical

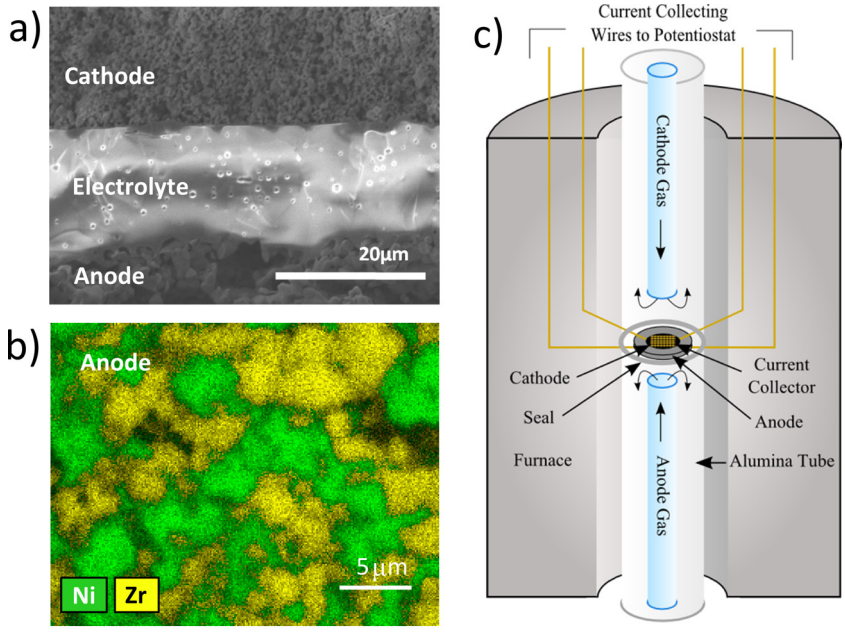

Fig. 1. (a) SEM image of the cross-section of the electrolyte of a fuel cell used in this study (b) Energy dispersive spectroscopy of the anode structure showing areas of nickel and zirconia (c) Diagram of the electrochemical testing setup.

measurements were performed using a PARSTAT 2273 (Princeton Applied Research) and included linear sweep voltammetry, electrochemical impedance spectroscopy, and constant voltage stability tests.

2.2. Catalyst characterization

2.2.1. Scanning electron microscopy

Electron micrographs were obtained using a Philips XL30FEG scanning electron microscope (SEM) which has a resolution of a few nanometers. We performed elemental analysis on the samples using a Si-Li solid state X-ray detector attached to this microscope which provided energy dispersive X-ray spectroscopy (EDS) data. Both the images and EDS data were collected with an accelerating voltage of 10 kV and a working distance of 10 mm. In all SEM experiments, the anode pellets were fractured down the middle of the cathode in order to obtain cross sections of the active fuel cell area.

2.2.2. X-ray photoelectron spectroscopy

X-ray photoelectron spectroscopy (XPS) data was taken using a Kratos Axis Ultra XPS with a monochromated alumina Kα source operating at 8 mA and 14 kV. Experiments were performed on fuel cell anode catalysts to determine the relative concentration of Sn and Ni in fresh and used materials. In all experiments, the charge neutralizer was used to prevent charging of the samples, and the carbon 1s peak at 284 eV was used to detect any shifting of the spectrum. The baseline for each spectrum was calculated using the Shirley algorithm, and peaks were fit and quantified for Ni, NiO and Sn using CasaXPS software.

2.3. Synthesis

Fig. 1 shows an SEM image of the cross section of a typical fuel cell, EDS mapping of the fuel cell anode, and the experimental setup used in this study. The planar fuel cell pellets were fabricated using yttria stabilized zirconia (YSZ) (8%, Tosoh), nickel oxide (NiO) (Alfa Aesar), and graphite (300 mesh, Alfa Aesar) powders in a weight ratio of 1:1:0.6. The powders were combined and ball-milled in de-ionized water for 24 h, and the resulting slurry was then dried and sifted. The powder was then pressed into 15 mm diameter pellets with a thickness of about 1 mm. The pellets were pre-fired at 1273 K for 4 h (2 K/min) to remove the carbon pore former. Solutions of $SnCl_2 \times 2H_2O$ in ethanol were added to the NiO/YSZ pellets using the incipient wetness technique to synthesize Sn/Ni anodes with a nominal Ni:Sn metal ratio of 100:1. The YSZ electrolyte was added drop wise to the surface of the pellets, suspended in a solution of ethanol and Ethocel-300 (Dow Chemical) and sintered at 1723 K for 4 h (1 K/min). The process resulted in the formation of the anode and electrolyte layers shown in Fig. 1a. The electrolyte layer of the fuel cells was 15–20 μm thick, while the anode layers were typically about 500 μm thick consisting of a mixture of irregularly shaped NiO (or NiO/Sn for the alloys) and YSZ particles which range from approximately 0.5 μm to 5 μm in diameter according to SEM images and EDS mapping shown in Fig. 1b. Two layers of cathode material were painted on the surface of the YSZ electrolyte in two steps using slurries ball-milled in ethanol for 24 h. The first layer had a weight ratio of 1:1 YSZ and lanthanum strontium manganite (LSM) ($La_{0.8}Sr_{0.2}Mn_{0.98}$, Praxair), and the second layer had a weight ratio of 0.25:1 graphite:LSM. The layers were sintered at 673 K and 1423 K for 2 h, respectively (2 K/min) creating a cathode layer about 50 μm thick. Gold mesh current collectors were secured to the cathode side using silver paste (Alfa Aesar), however gold mesh was not used on the anode side. Two gold wires were secured to each electrode using silver paste. The cells were secured to an alumina tube using alumina paste (Ceramabond 552) and placed in a furnace as shown in Fig. 1c. After curing the alumina paste, the temperature was ramped 0.8 K/min to 973 K in air, the system purged with Ar, and switched to hydrogen to reduce the NiO in the anode for 16 h. The cathode was left open to stagnant air during this process. The temperature was then brought up to the final fuel cell operating temperature.

3. Results

3.1. Electrochemical testing

Fig. 2 shows I–V and power curve data for monometallic Ni and 1% Sn/Ni cells after 10 min and 18–20 h operation on ethanol. In all experiments, fuel cells were first run on hydrogen at 120 sccm and a constant voltage of 0.6 V (voltage difference between anode and cathode) for 4–6 h. During this time, current density typically increased due to the activation of the cathode layer [29]. This operation on hydrogen allowed us to establish baseline activity for the fuel cell and to stabilize the cell operation. After this initial period, the fuel was switched from H_2 to 30 sccm argon bubbled through ethanol at room temperature (296 K). These conditions yield an ethanol vapor flow of approximately 2.2 sccm. The reported I–V curves and power data were taken by taking the cell to the open circuit voltage (OCV) and stepping down in voltage by 10 mV increments every 10 s from the OCV to 0.1 V. In all fuel cells, the initial OCV on hydrogen was between 1.05 and 1.08 V, which is close to the value predicted by the Nernst equation (∼1.1 V). When the fuel was switched to ethanol, the OCV decreased to 1.01–1.03 V. This decrease was expected, because the theoretical OCV for the conditions of our system was ∼1.04 V.

Fig. 2a shows I–V and power curve data for a monometallic Ni cell. The data suggests ethanol-induced changes in the performance of the cell over time. There are three observable differences in the data collected after 10 min and 18 h of operation: (i) at high voltages, close to the equilibrium voltage, a lower current is measured on the Ni cell operated for 18 h compared to the same cell operated for 10 min. This change in the I–V characteristics suggests ethanol-induced polarization losses, (ii) at the intermediate voltages (0.8 V–0.5 V), the slope of the I–V curve is smaller for the cell operated for 18 h compared to the same cell operated for 10 min, suggesting that the ohmic losses are smaller for the cell operated for longer time on ethanol, (iii) at low voltage, the cell operated for 18 h exhibits higher losses than the same cell operated for 10 min suggesting lower fuel mass transport rates after exposure to ethanol. All the observed changes in the I–V characteristics of the Ni cell can be explained by buildup of carbon deposits within the Ni anode. Carbon buildup lowers the concentration of active centers on Ni electrodes (thereby lowering the kinetic current measured at high voltage), improves the electronic contacts between neighboring Ni particles (therefore lowering ohmic resistance) [30], and lowers the rates of mass transport of the reactants by decreasing the porosity of the anode assembly. Fig. 2b shows the data for the 1% Sn/Ni cell operated under identical conditions as the Ni cell using ethanol fuel. The data show no significant changes in the performance of the cell over the 20 h of ethanol operation.

Fig. 3 shows I–V and power curve data collected for the similar monometallic Ni and 1% Sn/Ni cells while operating on hydrogen before and after exposure to ethanol, along with a control experiment where a monometallic Ni cell was operated only with hydrogen (this cell was never exposed to ethanol). Fig. 3a shows the I–V and power data from the control experiment where only hydrogen was used. The data show very little difference for data sets taken after 8 and 28 h of operation on hydrogen, suggesting that the fuel cell is stable over this period of time. Fig. 3b shows the I–V and power data for a monometallic Ni cell operated on hydrogen after the cell was exposed to 6 h of steady hydrogen operation (cir-

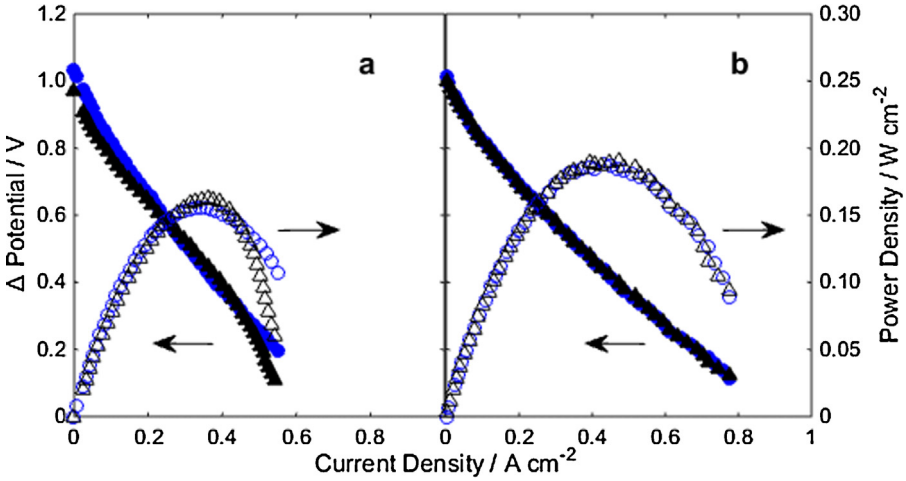

Fig. 2. I–V (solid markers) and power density (open markers) curves for fuel cells operated on 30 sccm Ar bubbled through ethanol at 296 K at 1013 K (a) monometallic Ni anode cell: circles are data collected after 10 min of operation on ethanol, triangles are data collected after 18 h operation on ethanol at 0.6 V (b) 1% Sn/Ni anode cell: circles are data collected after 10 min of operation on ethanol, triangles are data collected after 20 h operation on ethanol at 0.6 V.

cles) and after an additional 18 h of ethanol operation (triangles). The ethanol-induced changes in the hydrogen I–V data include a decrease in the current at high voltages and an increase in current at intermediate voltages. These changes are consistent to those reported in Fig. 2a, except that there are no significant changes at low voltage due to mass transport of the fuel. This is likely because hydrogen was fed in higher concentration and at a higher flow rate than ethanol which allowed for higher rates of hydrogen diffusion through the porous anode network. In addition, hydrogen is geometrically smaller than ethanol and its diffusion coefficient is inherently higher than that of ethanol. Fig. 3c shows the I–V and power data for a 1% Sn/Ni cell operated on hydrogen after the cell was exposed to 4 hrs of steady hydrogen consumption (circles) and after an additional 20 h of ethanol exposure. In contrast to Fig. 3b, the data in Fig. 3c shows that the 1% Sn/Ni cell is significantly more stable than the cell containing a monometallic Ni anode.

To further analyze electrochemical characteristics of the cells containing Ni and Sn/Ni anodes, we preformed potentiostatic impedance spectroscopy measurements. Fig. 4 shows Nyquist plots for the Ni cell operated only on hydrogen fuel as well as for the Ni and 1% Sn/Ni fuel cells operating on ethanol after 10 min and 18–20 h of operation at 0.6 V. The impedance measurements were collected at OCV with the voltage perturbation amplitude of 10 mV at frequencies ranging from 100 kHz to 100 mHz. In each Nyquist plot, there are two points where the data intercept the real axis (x axis). One point is at high frequency and low Zreal. This high frequency resistance is associated with ohmic losses, and it is attributed mainly to the electrolyte and the conductivity of the electrodes. The second x-axis intercept occurs at lower frequency and high Zreal. The x axis distance between these two x-axis intercept points is commonly referred to as the polarization resistance. It is attributed to polarization processes at the electrodes. We note that because the cells are anode supported with very thin electrolytes, no attempt was made to include a reference electrode and the polarization resistance contributions from the anode and cathode cannot be rigorously distinguished. We note that we do not expect significantly different changes on the cathodes for different cells since all the cells were exposed to air at identical conditions. Therefore, most of the differences in the changes in the polarization behavior of our devices can be attributed to the cell-specific changes in the anodes.

We first analyze the high frequency impedance (due to ohmic losses). We measure this impedance to be between 0.12 and 0.18 $\Omega\,cm^2$ for all tested cells. These values are consistent with the theoretical resistance of YSZ, which for the YSZ electrolyte thickness of 10–20 μm used in our experiments is predicted to be 0.08–0.16 $\Omega\,cm^2$ at 1013 K. The ohmic resistance decreases slightly over time for all cells which may be due to sintering of the

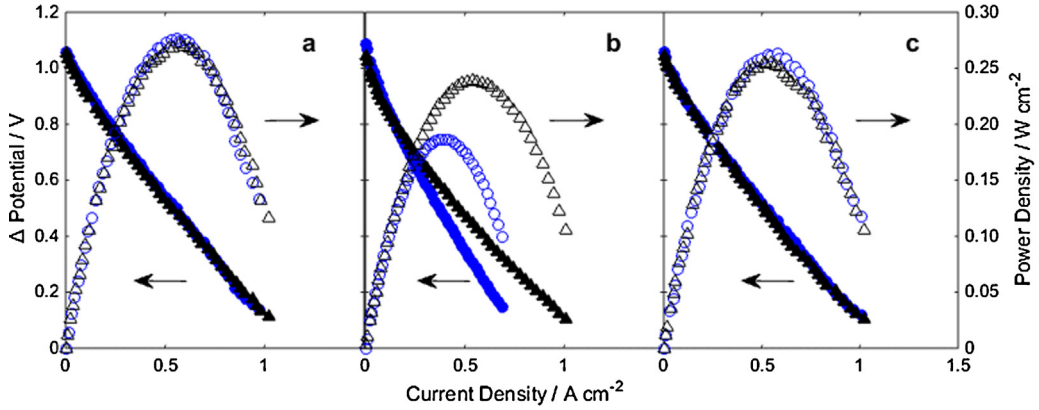

Fig. 3. I–V (solid markers) and power density (open markers) curves for fuel cells operated on 120 sccm hydrogen at 1013 K (a) Ni cell operated only on hydrogen: circles are data collected after 8 h at 0.6 V on hydrogen, triangles are data collected after 28 h at 0.6 V on hydrogen. (b) Ni cell operated on hydrogen: circles are data collected after 6 h at 0.6 V on hydrogen, triangles are data collected after 18 h at 0.6 V on ethanol. (c) 1% Sn/Ni cell operated on hydrogen: circles are data collected after 4 h at 0.6 V on hydrogen, triangles are data collected after 20 h at 0.6 V on ethanol.

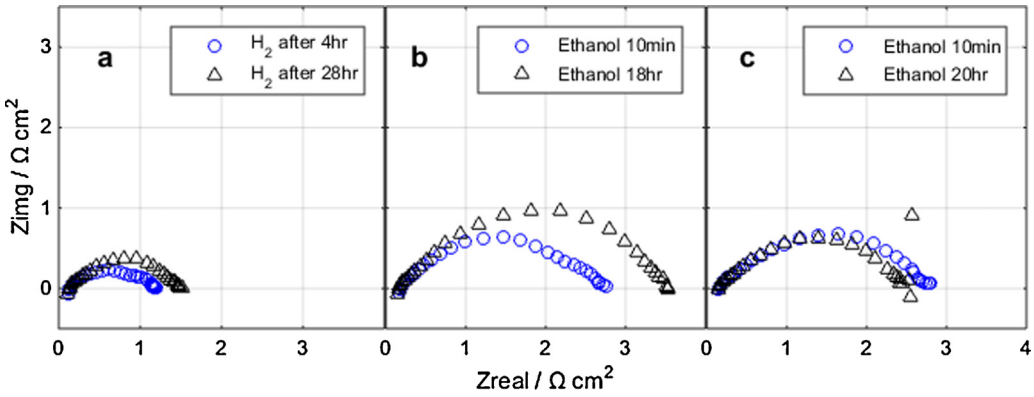

Fig. 4. Impedance spectroscopy taken at OCV and 1013 K. (a) Ni cell operated on only hydrogen: circles are data collected after 4 h at 0.6 V, triangles are data collected after 28 h at 0.6 V (b) Ni cell operated on ethanol: circles are data collected after 10 min at 0.6 V, triangles are data collected after 18 h at 0.6 V. (c) 1% Sn/Ni cell operated on ethanol: circles are data collected after 10 min at 0.6 V, triangles are data collected after 20 h at 0.6 V.

electrode particles which could increase the electrode conductivity and connection to the electrolyte. We note that larger decreases in the ohmic resistance are seen for the monometallic Ni cell operating on ethanol where the resistance decreases by about 10–14% after exposure to ethanol, as opposed to only 0–5% for the 1% Sn/Ni cell. This is most likely due to the carbon-induced increase in the electron conductivity on the anode side. Similar observations were reported by McIntosh et al. who showed large decreases in the ohmic resistance of their cells after exposure to carbon fuels, which they attributed to carbon increasing the conductivity of the anode as well as connecting previously isolated sections of the catalyst [30].

The data in Fig. 4 also show changes in the polarization resistance over time. Fig. 4a shows that the polarization resistance increased slightly over time for the monometallic Ni cells operated on hydrogen only. These increases are likely due to changes in the electrodes over time due to sintering on Ni particles, which causes a decrease in the catalytic surface area of the electrode. Fig. 4b shows that the polarization resistance also increases for the monometallic Ni cell operated on ethanol; however, this increase in the polarization resistance is much larger than the increase in Fig. 4a for the Ni cell that operated on hydrogen. The additional increase in the resistance is likely caused by carbon blocking active sites on the Ni anode surface. Fig. 4c shows that contrary to Ni, the polarization resistance decreased in the 1% Sn/Ni cell. This small decrease in the polarization resistance is likely caused by either a small loss or rearrangement of the Sn on the surface of the Ni. We have previously reported that while Sn aids the stability of the Ni electrodes, it also leads to a decrease in the inherent electrochemical activity of the Ni electro-catalysts. In Section 3.2 below we report XPS data which shows that some Sn has been lost from the surface of the anode particles after operation on ethanol fuel. We note that impedance spectroscopy measurements reported by Kan et al. on similar Sn/Ni systems in the electrochemical oxidation of alkanes showed a similar effect, and they also reported a small loss of Sn (~5%) from their system as measured by inductively coupled plasmon spectrometry (ICP) [28]. The lack of increase in the polarization resistance for the Sn/Ni anodes operated in ethanol is consistent with the observation that the rate of carbon deposition on the 1% Sn/Ni electrodes is significantly lower than on the Ni electrodes.

3.2. Ex-situ anode characterization

In addition to electrochemical testing, physical and chemical changes occurring in the SOFC anodes were analyzed ex-situ, using X-ray photoelectron spectroscopy (XPS) and scanning electron microscopy (SEM). Fig. 5 shows XPS data for the Ni 2p edge (Fig. 5a) and the Sn 3d edge (Fig. 5b) for three anode samples. As shown in the figure, the XPS data can be deconvoluted in terms of Ni, NiO, and Sn. The top spectra are data from a 1% Sn/Ni anode which was reduced in hydrogen at 973 K following the procedure identical to the one used before electrochemical testing. This anode was never operated as a fuel cell, and therefore is representative of the anode composition before exposure to ethanol. The middle spectra are data from the 1% Sn/Ni anode operated on ethanol for 20 h at 0.6 V and 1013 K, and the bottom spectra are data from the monometallic Ni anode that was operated on hydrogen at 0.6 V and 1013 K for 28 h. The Ni 2p data show that all samples contained a mixture of Ni and NiO surface domains. Sn 3d peaks were observed for the two 1% Sn/Ni anodes, however the Sn $3d_{3/2}$ peak is partially obstructed by an intense Auger Na KLL peak (this is an impurity due to the sample and holder handling). Further analysis of the XPS spectra aimed at quantifying the relative concentration of Sn and Ni at the surface of the electro-catalytic particles demonstrated that for the nominal, bulk Sn loading of 1%, the surface concentration of Sn was approximately 3% (this is the concentration detected by XPS). This enrichment of Sn at the surface has been observed before and it is a consequence of the thermodynamically preferred Sn enrichment at the surface layers of Ni particles [31]. The analysis also showed that the Sn content in the surface of the particles was depleted to 1.8% after operation on ethanol for 20 h.

To further investigate the composition of the material, the used cells were fractured and the cross-sections were imaged using SEM with an EDS detector. Fig. 6 shows SEM images and corresponding EDS maps of Ni and 1% Sn/Ni fuel cells obtained for the regions ~100 μm from the outer edge of the anode (~400 μm from the electrolyte). Fig. 6a shows an SEM image of a Ni/YSZ anode that has operated on hydrogen for 28 h at 0.6 V. Fig. 6b shows the corresponding EDS map. These images provide a baseline to compare to the cells run on ethanol. The Ni particles obtained after the cell was operated on hydrogen are smooth and the map shows only large areas occupied by Ni and Zr. Fig. 6c and d shows the SEM image and EDS map for the Ni cell after operation on ethanol for 18 h at 0.6 V. The SEM image shows many regions where the Ni and YSZ particles appear rough and broken apart. These regions correspond to areas occupied by carbon in the EDS map. Fig. 6e and f shows images for the 1% Sn/Ni cell after operation on ethanol for 20 h at 0.6 V. The SEM image shows mainly smooth particles, and the EDS map indicates only a few small areas of carbon buildup.

Although the SEM images provide good visualization of the degradation and carbon deposition on the anode surface, SEM can only provide images of small areas which may not be representative of the overall anode structure. Therefore, in addition to the imaging and mapping of the carbon deposits within the fuel cells,

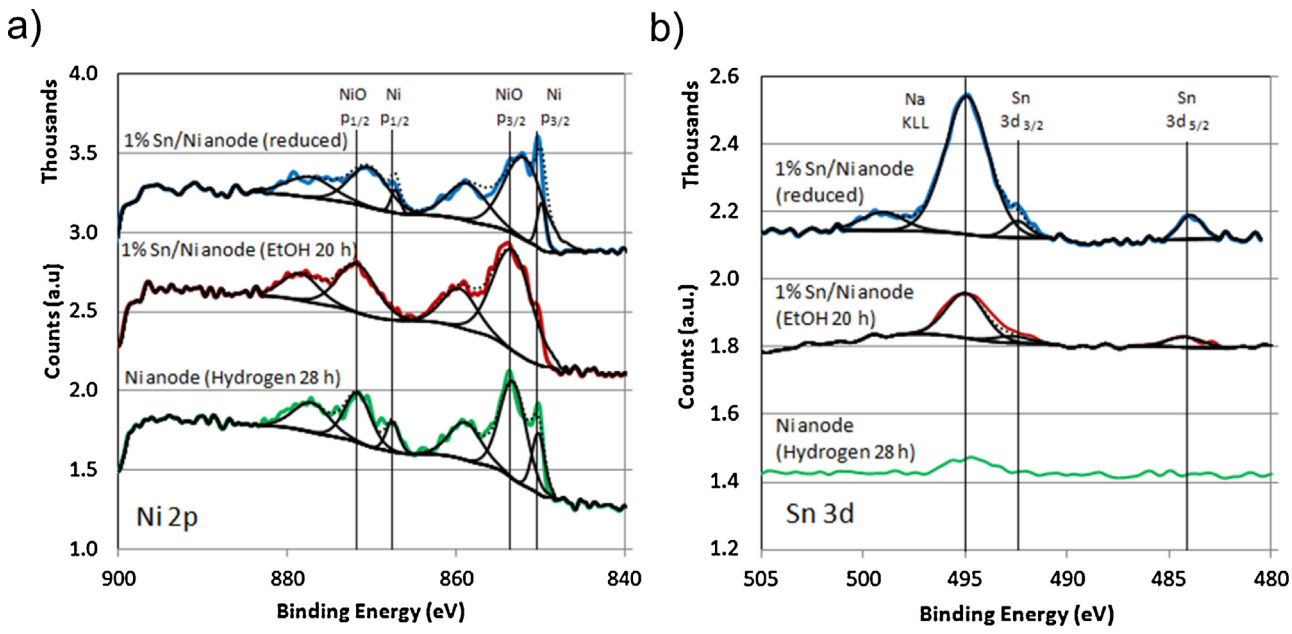

Fig. 5. XPS data and curve fitting for (a) the Ni 2p edge and (b) the Sn 3d edge.

we have also used EDS to quantify where the carbon deposits are concentrated within the anode. Fig. 7 shows the ratio of the C to Ni EDS signals (C/Ni peak ratio) obtained at several distances from the electrolyte for fuel cells operating at several different conditions. The C/Ni peak ratios were averaged over several points along the electrolyte to give a better indication of the carbon deposition over a larger fuel cell area. Spectra were taken approximately every 50 μm along lines orthogonal to the electrolyte. A fuel cell operated on only hydrogen is included with the data to indicate a baseline for comparison of C/Ni peak ratios of the other fuel cells. In the figure, a C/Ni peak ratio larger than the baseline indicates carbon deposition. Overall, three major trends can be observed from Fig. 7. First, carbon deposition is most severe at the outer edge of the anode, furthest from the electrolyte. This is shown in Fig. 7 as an increase in C/Ni peak ratios as distance from the electrolyte increases. This is not surprising since the outer edge of the anode is exposed to the highest carbon concentration from the fuel, and the lowest concentration of oxygen from the electrolyte, causing higher carbon deposition on the outer edge of the anode. The second trend is that the operating voltage has a large effect on the carbon deposition on the anode surface. Fig. 7 shows that after cell operation on ethanol at 0.5 V for 18 h, there is very little carbon detected. Similarly, even smaller amounts of carbon were detected in the 1% Sn/Ni cell after 18 h of exposure to ethanol at 0.5 V. At 0.6 V, there is carbon detected at the outer edge of both the monometallic and 1% Sn/Ni cells. This is also not surprising since a lower ΔV results in higher current which means that the rate of the transport of oxygen ions through the electrolyte is higher, indicating that effective O/C

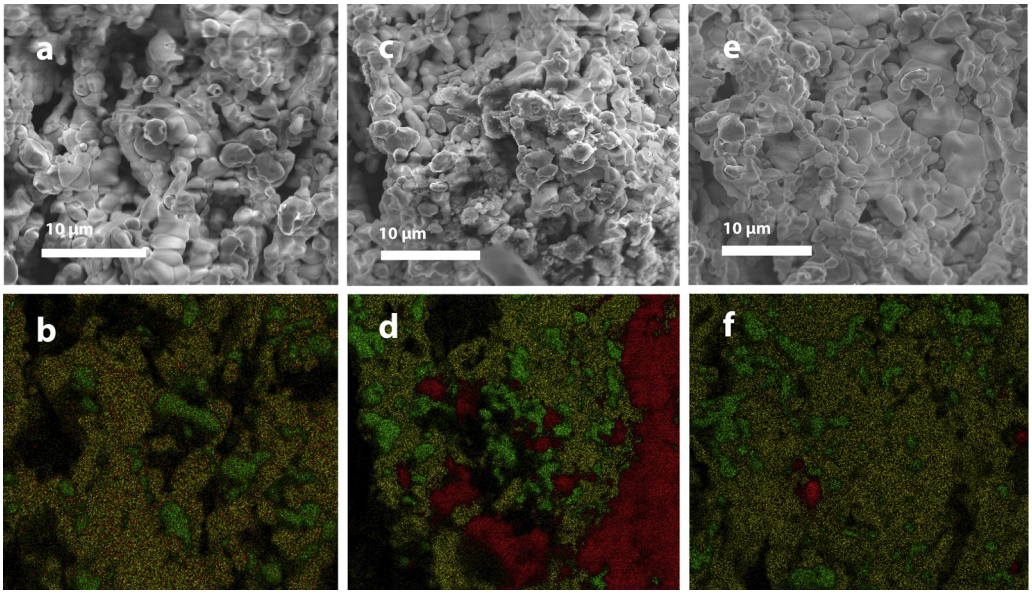

Fig. 6. SEM images (top) with EDS maps (bottom) taken 100 μm from the outside of the anode showing Ni (green), Zr (yellow) and C (red) for (a, b) Ni anode fuel cell operated on only H_2 for 28 h (c, d) Ni anode fuel cell operated on ethanol at 0.6 V for 18 h (e, f) 1% Sn/Ni anode fuel cell operated on ethanol at 0.6 V for 20 h.(For interpretation of the references to colour in this figure legend, the reader is referred to the web version of this article.)

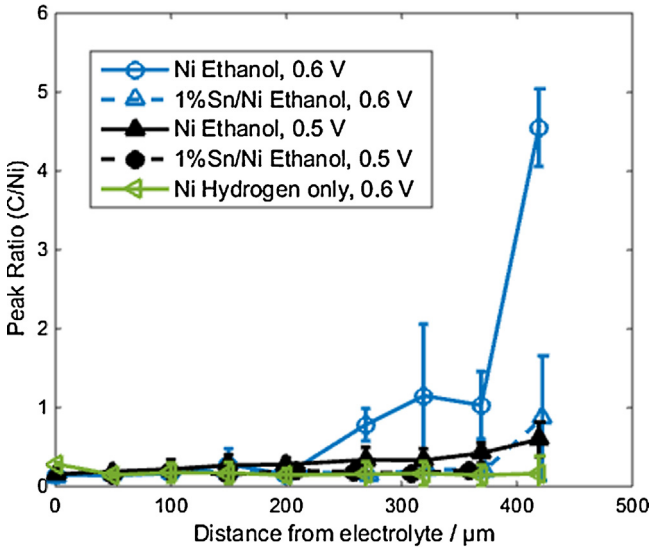

Fig. 7. EDS C/Ni peak ratios for fuel cells as a function of distance from the electrolyte. The final measurement for each cell is taken 50 μm from the outer edge of the anode.

ratio is higher at lower ΔV. Finally, for all tested cells, the cells that employed the 1% Sn/Ni anodes exhibited less carbon deposition than the cell with monometallic Ni anodes operating at identical conditions. This is most apparent in the data from the cells operated at 0.6 V, where the 1% Sn/Ni cell only has a relatively small amount of carbon detected at 50 μm from its outer edge. In contrast, for the Ni cell operating at similar conditions, carbon is detected 200 μm from the outer edge of the cell, with very large amounts of carbon near the outer edge.

4. Discussion

The data discussed above showed that the introduction of small amounts of Sn to Ni anode electro-catalysts enhances the stability of the anode to carbon-induced deactivation over a range of operating conditions when oxygenated hydrocarbons such as ethanol are employed as fuels. This was demonstrated through the observations that after exposure to ethanol, the cells fabricated with monometallic Ni anodes showed decreased current densities at high voltages, and increased polarization resistance at OCV. Both of these effects are likely due to carbon blocking of the active sites at the surface of the electro-catalyst particles. We have previously reported similar findings for the Ni-based anodes operating on methane and iso-octane [14]. These previous studies included a detailed characterization of the anode electro-catalysts which suggested that Sn atoms preferentially segregate to the under-coordinated sites on the surface of Ni electro-catalyst nanoparticles, eliminating nucleation sites for carbon growth [11,32]. Furthermore, it was postulated that Sn atoms break up the ensembles of the surface Ni atoms that are required for the formation of extended carbon planar networks and filaments [26,32]. Since the Ni and Sn/Ni anode electro-catalysts employed in this study are identical to those used previously, we postulate that the underlying molecular mechanisms associated with the observed extended lifetime of the Sn/Ni anode electro-catalysts are identical, and that they include the Sn-induced changes in the carbon chemistry of Ni surfaces [14,25,26,31,32].

The studies above also shed light on a few critical guiding principles that need to be considered when designing SOFC systems that utilize hydrocarbons or bio-derived oxygenated hydrocarbons fuels. First, it has to be recognized that there are many chemical and electro-chemical reactions that are taking place in the anode compartment when these fuels are fed directly to the cell. The nature of these reactions and the regions of anode compartments where they are dominant are heavily influenced by the local oxygen (including O^{2-} ions) to fuel ratios. For example, at the three-phase-boundary (TPB), where electrolyte and anode electro-catalysts are in contact with each other, due to high activity of oxygen ions (which is the result of high transport rates through the electrolyte), deep and partial electrochemical oxidation reactions will dominate. These reactions are not the source of the formation of carbon deposits, as illustrated in Fig. 7. On the other hand in the regions away from the TPB, steam and dry reforming of the fuel that involve water and CO_2 respectively take place. We note that water and CO_2 are produced at the TPB boundary during the electrochemical oxidation process. These reforming reactions could result in the formation of carbon deposits. In addition, even further from the electrolyte where oxygen content is depleted even more, hydrocarbon pyrolysis reactions take place. For oxygenated hydrocarbons such as ethanol at the operating temperature of 1013 K, the process of pyrolysis results in the formation of CO, CO_2, CH_4, ethylene, ethane, and hydrogen. While some of these compounds are excellent fuels for SOFCs, others are very potent in forming carbon deposits in the anode. For example, ethylene has been shown to rapidly build graphitic carbon deposits on Ni catalyst surfaces [15]. This is supported by Fig. 7 which shows that the extent of carbon deposition increases for the regions farther away from the electrolyte.

If the process of carbon deposition is to be limited, it is imperative to design anodes that operate with high oxygen to carbon ratios. Therefore, thin membranes that are excellent ion conductors are preferred. Furthermore, since the activity of oxygen is the highest at the TPB, it is important to increase the ratio of the TPB surface to the volume of the anode compartment. Even if these design principles are embraced, there will be reforming and pyrolysis reactions taking place at the elevated SOFC operating temperatures. As discussed above, these reactions can lead to rapid degradation of conventional Ni anode electro-catalysts. In this case, significant reductions in the rates of formation of carbon deposits can be achieved by designing electro-catalysts, such as the above discussed Sn/Ni alloy, that have lower propensity to activate the formation of carbon deposits compared to monometallic Ni without significant reduction of the reaction rates. It is important to point out that even when these catalysts are employed, if the local oxygen to carbon ratio is exceedingly low (below the stoichiometric limit for the formation of CO), the carbon deposition cannot be prevented and the cell will eventually accumulate carbon and deactivate.

5. Conclusions

We have demonstrated that carbon deposition catalyzed on monometallic Ni in the process of electrochemical oxidation of oxygenated hydrocarbon fuels (e.g., ethanol) can be decreased by Ni alloying with small amounts of Sn. In SOFCs fabricated using monometallic Ni, carbon deposition resulted in physical and electrochemical changes to the Ni anode. In contrast, Sn/Ni alloy anodes inhibited the formation of carbon-induced degradation catalyzed by Ni, resulting in smaller electrochemical changes over time and less carbon deposition. Additionally, we have shown that carbon deposition is affected by the location of the catalyst in the anode as well as the operating voltage, which are both factors that affect the local C/O ratio on the catalyst surface. Overall our results indicate that the catalyst surface chemistry and local C/O ratios are both important factors that must be considered in the design of fuel cell anode catalysts operating on oxygenated hydrocarbon fuels.

Acknowledgements

We gratefully acknowledge support from United States Department of Energy, Office of Basic Energy Science, Division of Chemical Sciences (FG-02-05ER15686). B.F. acknowledges that this material is based upon work supported by the National Science Foundation Graduate Research Fellowship under Grant No. DGE 1256260.

References

[1] R.M. Ormerod, Solid oxide fuel cells, Chem. Soc. Rev. 32 (2003) 17–28, http://dx.doi.org/10.1039/b105764m.
[2] E.D. Wachsman, C.A. Marlowe, K.T. Lee, Role of solid oxide fuel cells in a balanced energy strategy, Energy Environ. Sci. 5 (2012) 5498–5509, http://dx.doi.org/10.1039/c1ee02445k.
[3] A. Atkinson, S. Barnett, R.J. Gorte, J.T.S. Irvine, A.J. McEvoy, M. Mogensen, et al., Advanced anodes for high-temperature fuel cells, Nat. Mater. 3 (2004) 17–27, http://dx.doi.org/10.1038/nmat1040.
[4] T.A. Adams II, P.I. Barton, High-efficiency power production from coal with carbon capture, Process Syst. Eng. 56 (2010) 3120–3136, http://dx.doi.org/10.1002/aic.
[5] T.A. Adams II, P.I. Barton, High-efficiency power production from natural gas with carbon capture, J. Power Sources 195 (2010) 1971–1983, http://dx.doi.org/10.1016/j.jpowsour.2009.10.046.
[6] D.D. Hsu, D. Inman, G.A. Heath, E.J. Wolfrum, M.K. Mann, A. Aden, Life cycle environmental impacts of selected U.S. ethanol production and use pathways in 2022, Environ. Sci. Technol. 44 (2010) 5289–5297, http://dx.doi.org/10.1021/es100186h.
[7] H. Wu, M. Wang, M. Liu, J. Huo, Life-cycle assessment of corn-based butanol as a potential transportation fuel, (2007).
[8] R.J. Gorte, J.M. Vohs, Catalysis in solid oxide fuel cells, Annu. Rev. Chem. Biomol. Eng. 2 (2011) 9–30, http://dx.doi.org/10.1146/annurev-chembioeng-061010-114148.
[9] S. McIntosh, R.J. Gorte, Direct hydrocarbon solid oxide fuel cells, Chem. Rev. 104 (2004) 4845–4866, http://www.ncbi.nlm.nih.gov/pubmed/15669170.
[10] S. Park, J.M. Vohs, R.J. Gorte, Direct oxidation of hydrocarbons in a solid-oxide fuel cell, Nature 404 (2000) 265–267, http://dx.doi.org/10.1038/35005040.
[11] S. Helveg, C. Lopez-Cartes, J. Sehested, P.L. Hansen, B.S. Clausen, J.R. Rostrup-Nielsen, et al., Atomic-scale imaging of carbon nanofibre growth, Nature 427 (2004) 426–429, http://dx.doi.org/10.1038/nature02308.1.
[12] Y. Kim, J.H. Kim, J. Bae, C.W. Yoon, S.W. Nam, In situ analyses of carbon dissolution into Ni-YSZ anode materials, J. Phys. Chem. C 116 (2012) 13281–13288, http://dx.doi.org/10.1021/jp3035693.
[13] K.S. Blinn, H. Abernathy, X. Li, M. Liu, L.A. Bottomley, M. Liu, Raman spectroscopic monitoring of carbon deposition on hydrocarbon-fed solid oxide fuel cell anodes, Energy Environ. Sci. 5 (2012) 7913–7917, http://dx.doi.org/10.1039/c2ee21499g.
[14] E. Nikolla, J. Schwank, S. Linic, Direct electrochemical oxidation of hydrocarbon fuels on SOFCs: improved carbon tolerance of ni alloy anodes, J. Electrochem. Soc. 156 (2009) B1312–B1316, http://dx.doi.org/10.1149/1.3208060.
[15] M.B. Pomfret, J. Marda, G.S. Jackson, B.W. Eichhorn, A.M. Dean, R.A. Walker, Hydrocarbon fuels in solid oxide fuel cells: in situ raman studies of graphite formation and oxidation, J. Phys. Chem. C 112 (2008) 5232–5240, http://dx.doi.org/10.1021/jp711312p.'
[16] M.B. Pomfret, D.A. Steinhurst, J.C. Owrutsky, Methanol and ethanol fuels in solid oxide fuel cells: a thermal imaging study of carbon deposition, Energy Fuels 25 (2011) 2633–2642, http://dx.doi.org/10.1021/ef2003975.
[17] B.C. Eigenbrodt, J.D. Kirtley, R.A. Walker, In-situ optical studies of solid oxide fuelcell operating with dry and humidified oxygenated fuels, ECS Trans. 35 (2011) 2789–2798.
[18] M.B. Pomfret, J.C. Owrutsky, R.A. Walker, High-temperature Raman spectroscopy of solid oxide fuel cell materials and processes, J. Phys. Chem. B 110 (2006) 17305–17308, http://dx.doi.org/10.1021/jp063952l.
[19] K. Sasaki, K. Watanabe, Y. Teraoka, Direct-alcohol SOFCs: current–voltage characteristics and fuel gas compositions, J. Electrochem. Soc. 151 (2004) A965–A970, http://dx.doi.org/10.1149/1.1756884.
[20] M. Younessi-Sinaki, E.A. Matida, F. Hamdullahpur, Kinetic model of homogeneous thermal decomposition of methane and ethane, Int. J. Hydrogen Energy 34 (2009) 3710–3716, http://dx.doi.org/10.1016/j.ijhydene.2009.03.014.
[21] S.D. Nobrega, M.V. Galesco, K. Girona, D.Z. de Florio, M.C. Steil, S. Georges, et al., Direct ethanol solid oxide fuel cell operating in gradual internal reforming, J. Power Sources 213 (2012) 156–159, http://dx.doi.org/10.1016/j.jpowsour.2012.03.104.
[22] X.-F. Ye, S.R. Wang, Q. Hu, Z.R. Wang, T.L. Wen, Z.Y. Wen, Improvement of multi-layer anode for direct ethanol solid oxide fuel cells, Electrochem. Commun 11 (2009) 823–826, http://dx.doi.org/10.1016/j.elecom.2009.02.003.
[23] K. Sasaki, Y. Teraoka, Equilibria in fuel cell gases II, J. Electrochem. Soc. 150 (2003) A885–A888, http://dx.doi.org/10.1149/1.1577338.
[24] K. Sasaki, Y. Teraoka, Equilibria in fuel cell gases I, J. Electrochem. Soc. 150 (2003) A878–A884, http://dx.doi.org/10.1149/1.1577338.
[25] E. Nikolla, J. Schwank, S. Linic, Hydrocarbon steam reforming on Ni alloys at solid oxide fuel cell operating conditions, Catal. Today 136 (2008) 243–248, http://dx.doi.org/10.1016/j.cattod.2008.03.028.
[26] E. Nikolla, J. Schwank, S. Linic, Comparative study of the kinetics of methane steam reforming on supported Ni and Sn/Ni alloy catalysts: the impact of the formation of Ni alloy on chemistry, J. Catal. 263 (2009) 220–227, http://dx.doi.org/10.1016/j.jcat.2009.02.006.
[27] D. Yoon, A. Manthiram, Hydrocarbon-fueled solid oxide fuel cells with, J. Mater. Chem. A. 2 (2014) 17041–17046, http://dx.doi.org/10.1039/C4TA02662D.
[28] H. Kan, H. Lee, Sn-doped Ni/YSZ anode catalysts with enhanced carbon deposition resistance for an intermediate temperature SOFC, Appl. Catal. B Environ. 97 (2010) 108–114, http://dx.doi.org/10.1016/j.apcatb.2010.03.029.
[29] Y. Leng, Performance evaluation of anode-supported solid oxide fuel cells with thin film YSZ electrolyte, Int. J. Hydrogen Energy 29 (2004) 1025–1033, http://dx.doi.org/10.1016/j.ijhydene.2004.01.009.
[30] S. McIntosh, J.M. Vohs, R.J. Gorte, Role of hydrocarbon deposits in the enhanced performance of direct-oxidation SOFCs, J. Electrochem. Soc. 150 (2003) A470–A476, http://dx.doi.org/10.1149/1.1559064.
[31] E. Nikolla, J. Schwank, S. Linic, Promotion of the long-term stability of reforming Ni catalysts by surface alloying, J. Catal. 250 (2007) 85–93, http://dx.doi.org/10.1016/j.jcat.2007.04.020.
[32] E. Nikolla, A. Holewinski, J. Schwank, S. Linic, Controlling carbon surface chemistry by alloying: carbon tolerant reforming catalyst, J. Am. Chem. Soc. 128 (2006) 11354–11355, http://dx.doi.org/10.1021/ja0638298.